Strong bulk spin-orbit torques quantified in the van der Waals ferromagnet Fe_3GeTe_2

Franziska Martin[1], Kyujoon Lee[1,2,], Maurice Schmitt[1], Anna Liedtke[1], Aga Shahee[1], Haakon Thømt Simensen[3], Tanja Scholz[4], Tom G. Saunderson[1], Dongwook Go[1,5], Martin Gradhand[1,6], Yuriy Mokrousov[1,5], Thibaud Denneulin[7], András Kovács[7], Bettina Lotsch[4], Arne Brataas[3], Mathias Kläui[1,3]*

[1]Institute of Physics, Johannes Gutenberg-University, 55099 Mainz, Germany

[2]Division of Display and Semiconductor Physics, Korea University, 30019 Sejong, Korea

[3]Centre for Quantum Spintronics, Department of Physics, Norwegian University of Science and Technology, 7491 Trondheim, Norway

[4]Max Planck Institute for solid state research, 70569 Stuttgart, Germany

[5]Peter Grünberg Institut and Institute for Advanced Simulation, Forschungszentrum Jülich and JARA, 52425 Jülich, Germany

[6]H. H. Wills Physics Laboratory, University of Bristol, Bristol BS8 1TL, United Kingdom

[7]Ernst Ruska-Centre for Microscopy and Spectroscopy with Electrons and Peter Grünberg Institute, Forschungszentrum Jülich, 52425 Jülich, Germany

[*]Author to whom correspondence should be addressed: lkjoon@korea.ac.kr

Keywords: Van der Waals, two-dimensional magnet, spin-orbit torque

Abstract

The recent emergence of magnetic van der Waals materials allows for the investigation of current induced magnetization manipulation in two dimensional materials. Uniquely, Fe_3GeTe_2 has a crystalline structure that allows for the presence of *bulk* spin-orbit torques (SOTs) that we quantify in a Fe_3GeTe_2 flake. From the symmetry of the measured torques, we identify current induced effective fields using harmonic analysis and find dominant *bulk* SOTs arising from the symmetry in the crystal structure. Our results show that Fe_3GeTe_2 can exhibit *bulk* SOTs in addition to the conventional interfacial SOTs enabling magnetization manipulation even in thick flakes without the need for complex multilayer engineering.

1. Introduction

The discovery of magnetic van der Waals crystals that retain magnetic order in the two-dimensional limit [1–4] opens up the investigation of their magnetic properties and implementation in spintronic devices. Consequently, the efficient control of the magnetic state is essential. Spin-orbit torques (SOTs) provide the opportunity of electrical control of magnetizations [5]. Linking magnetic van der Waals materials with SOTs potentially allows for two dimensional current induced magnetization manipulation enabling fast, low power spintronic devices. So far reports of current-induced switching of 2D magnets have been based on interfacial SOTs in complex multilayers requiring small magnetic layer thicknesses, limiting thermal stability.[6–8] One of the promising magnetic van der Waals crystals, Fe_3GeTe_2, has been shown to exhibit strong perpendicular magnetocrystalline anisotropies [9] present even in an atomic monolayer [10]. This, combined with the Dzyaloshinskii-Moriya interaction, also stabilizes skyrmions [11–13]. Furthermore, of the van der Waals materials it shows one of the highest bulk Curie temperatures of ~ 225 K [9,14] which can be increased up to room temperature by ionic gating [15].

While switching due to interfacial spin-orbit torques in Fe_3GeTe_2 has been studied in multilayer structures, Johansen et al. [16] recently predicted that a possible *bulk* SOT could be present due to the symmetry of the monolayer crystalline structure. Since Fe_3GeTe_2 is a metal, the combination of the perpendicular magnetic anisotropy with this theoretically predicted *bulk* SOTs could potentially enable simple new devices: *bulk* SOTs are efficient for thick samples that have a better magnetic thermal stability than the thin flakes necessary for interfacial SOTs, while also drastically simplifying single layer device engineering. However, symmetry analysis has so far only indicated *bulk* SOTs are allowed by symmetry [16], but the torques in single Fe_3GeTe_2 layers have not been quantified. Although there have been demonstrations of bulk-type SOTs in 3D magnets such as $L1_0$ FePt and Co-Tb, the origin and the behavior of the SOTs are different from the special *bulk* SOTs that are only present in

materials with particular crystalline structure as studied here in Fe_3GeTe_2[17,18]. Subsequently there is clear need to check the presence, identify the origin and quantify the amplitude of the torques as key steps forward. In this work, we measure the current induced effective spin-orbit fields in Fe_3GeTe_2. We analyze the symmetries and amplitudes of the torques to understand the bulk and interfacial contributions to the torques and ascertain the temperature dependence highlighting exceptionally large bulk torques in this system.

2. Results and discussion

Bulk single crystal Fe_3GeTe_2 was grown by chemical vapor transport (see Supplementary methods). The atomic structure was verified using high-resolution scanning transmission electron microscopy in Fig. S1a (see also Supplementary Note 1 and 7). We confirmed the stoichiometric composition of the Fe_3GeTe_2 by energy dispersive X-ray spectroscopy within an error of about 5% (see Supplementary Note 2). Subsequent high resolution transmission electron microscopy (see Supplementary Note 7) and field and temperature dependence of magnetisation (see Supplementary Notes 8,9) also confirm this. From the grown bulk crystals, Fe_3GeTe_2 flakes were manually exfoliated and placed on an undoped naturally oxidized silicon substrate. The thickness of the flake was measured with an atomic force microscope (Supplementary Note 10). By using electron beam lithography, gold contacts were fabricated. The final device can be seen in the inset of Fig. 1a. The flake used in the following study is measured to be 35 nm thick. Assuming the current flows between the transverse contacts, the cross-section area of the investigated flake is estimated to $A = 1.75 \times 10^{-13}$ m^2, which is the value used to calculate the current densities.

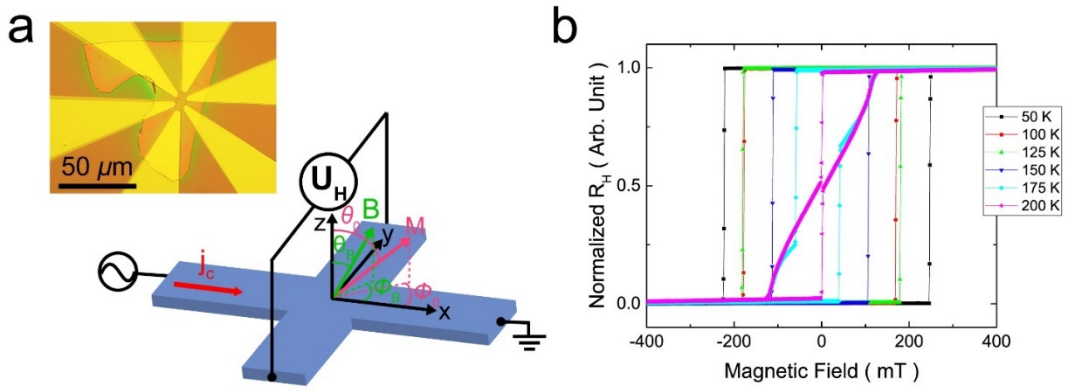

Figure 1. (a) Scheme of the 2nd harmonic Hall measurement. An alternating current is injected along the *x*-direction, while the transverse 1st and 2nd harmonic Hall voltage U_{trans} is measured via a lock-in amplifier. In the inset an optical microscope image of the final device is depicted. (b) The hysteresis loops of Fe_3GeTe_2 at different temperatures with the magnetic field applied in the z direction.

In order to measure the SOTs, higher harmonic Hall measurements [19] are performed. The measurements were done with the configuration shown in Fig. 1a where the current was applied in the *x* direction and the Hall voltage U_H was measured in the *y* direction. The perpendicular magnetic anisotropy of the flake was confirmed by the anomalous Hall measurements for different temperatures as shown in Fig. 1b. While at low temperature abrupt switching is seen, a multi-step switching appears above 175 K near T_c which shows a formation of domains and even skyrmions as observed by TEM in Fig. S4 (supplementary Note 4). At various temperatures and applied alternating currents j_C, the first (U_H^{1st}) and second harmonic (U_H^{2nd}) Hall voltages are recorded using lock-in amplifiers. For each combination of temperature and current, a magnetic field **B** is applied in the plane to tilt the magnetization **M**. Thereby, the external field is either aligned with the longitudinal current direction ($\Phi B = 0°$) or perpendicular to it ($\Phi_B = 90°$). A small z-component prevents multi-domain nucleation, so that the polar angle of the external field ranges between $80° \leq \theta_B \leq 83°$. To take care of heating effects, the second harmonic signal is corrected according to the method outlined in [19].

To extract the SOT effective fields the measured first and second harmonic voltages were analyzed in supplementary Note 5. In Ref. [16] the current induced effective spin-orbit field has been derived for the Fe_3GeTe_2 crystal structure:

$$\boldsymbol{B}_{SOT} = \Gamma_0 J_C (m_x \boldsymbol{e}_x - m_y \boldsymbol{e}_y) \quad (1)$$

Γ_0 is a parameter, which represents the strength of the SOTs, J_C is the applied current density, m_i is the i^{th} component of the magnetization unit vector and $\mathbf{e}_x$ and $\mathbf{e}_y$ are the x- and y-unit vectors. We see that these torques lead to a canting of the spins into the plane of the sample and can facilitate switching by reducing the switching energy barrier. The canting lends itself naturally to detection by higher harmonic Hall measurements. By transforming equation (1) to spherical coordinates and considering the measurement configuration $\Phi = 0°/90°$, we find that the spin-orbit field only comprises a θ-component:

$$B_\theta^{SOT} = \Gamma_0 J_0 / 2 \sin(\theta_0) \cos(2\Phi) \quad (2)$$

$J_0 = j_0/A$ is the current density. For this reason, b^{Φ}_{SOT} in equation (S4) is also zero and the first and second harmonic Hall resistances can finally be formulated to:

$$R_H^{1st} = R_{AHE} \cos(\theta_0) \quad (3)$$

$$R_H^{2nd} = j_0/2 R_{AHE} \frac{\partial \cos(\theta)}{\partial B}\Big|_{\theta 0} \frac{1}{\sin(\theta_B - \theta_0)} b_{SOT}^{\theta} \quad (4)$$

Consequently, by measuring R_H^{2nd}, θ_0 and $R_{AHE} \frac{\partial \cos(\theta)}{\partial B}\Big|_{\theta 0} = \frac{\partial R H^{1st}}{\partial B}\Big|_{\theta 0}$, we derive the current induced effective SOTs b^{θ}_{SOT}. In Fig. 2 the first and second harmonic Hall resistances after correction for heating effects are plotted as a function of the applied magnetic field when the magnetic field applied in the $\Phi = 0°$ and 90° direction. Note that the field dependence of the second harmonic signal in the $\Phi = 0°$ and 90° configurations is found to be odd and even, respectively.

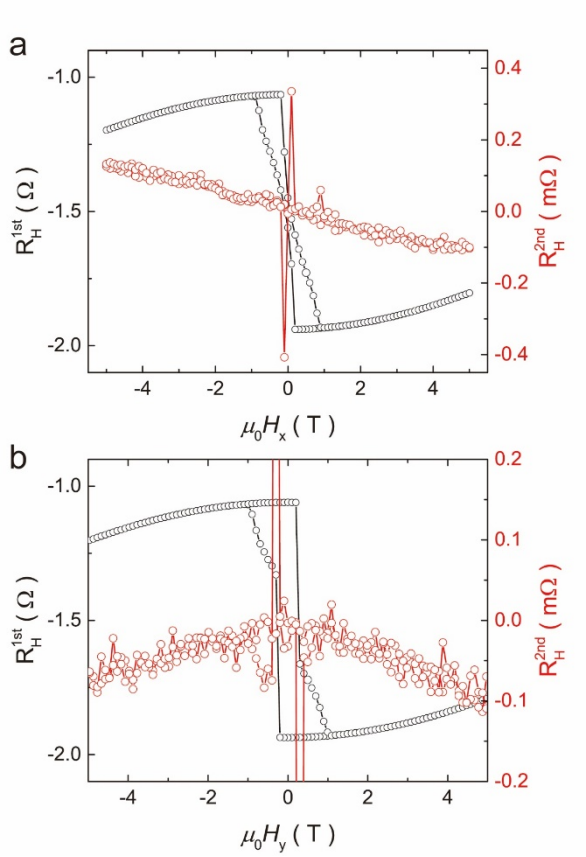

Figure 2. Examples of the 1st and 2nd harmonic Hall resistances as a function of the applied magnetic field along the *x*-direction $\Phi = 0°$ (a) and y-direction $\Phi = 90°$ (b) at a temperature of 100 K with a polar magnetic field angle of $\theta_B = 82°$. The applied current density is 4.1×10^{10} Am^{-2}.

The next step is to check the nature of the torques by measuring their symmetry. To obtain the polar angular dependence (θ_0), we plot in Fig. 3a the current-induced effective SOT b^{θ}_{SOT} as a function of applied magnetic field, corresponding to a certain polar angle. Data points from smaller external fields are omitted, due to the term $\frac{\partial RH^{1st}}{\partial B}\Big|_{\theta 0}$ diverging near the switching region. In Fig. 3b the same b^{θ}_{SOT} data is plotted as a function of the extracted polar magnetization angle θ_0. To demonstrate the odd-symmetry dependence of the damping-like effective field geometry ($\Phi = 0°$) and check that they overlap, we invert the data points corresponding to negative applied fields. The field-like effective field geometry ($\Phi = 90°$) values range between -2 and 4 mT/10^{11} Am^{-2} with the highest values at smaller θ_0 angles. The

damping-like effective fields decrease in magnitude from -8 to -3 mT/10^{11} Am^{-2} with increasing angle. Above θ_0 > 45° the absolute value of b^{θ}_{SOT} increases again up to -4 mT/10^{11} Am^{-2}.

The key step now is to clarify the origin of these torques to check if they are of bulk origin as predicted. A first observed key feature that allows us to identify the bulk origin is the opposite behaviour of the effective spin-orbit fields for Φ = 0° and Φ = 90° as predicted by equation (2) due to the cos(2Φ) term that yields +1 for Φ = 0° and –1 for Φ = 90°.

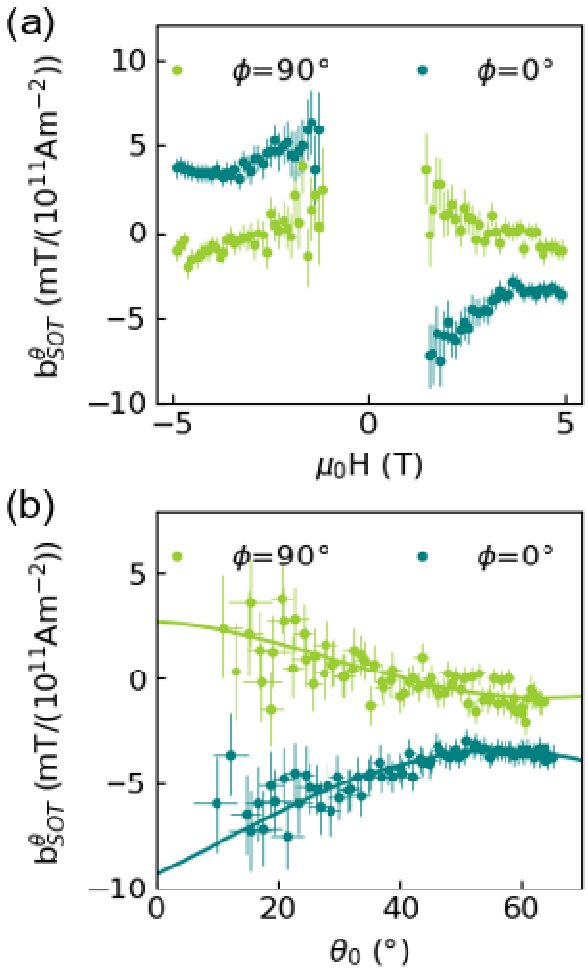

Figure 3. The derivative of the θ component of the current induced effective field is shown as a function of the externally applied magnetic field (a) and polar magnetization angle θ_0 (b) at a temperature of 175 K with a polar magnetic field angle of θ_B = 82°. The applied current density is 3.7 × 10^{10} Am^{-2}. In (b) the data for Φ = 0° and negative applied fields has been inverted. The solid lines are fits according to equations (5) and (6).

Secondly, from the θ_0 dependence we identify a dominating bulk origin. We fit equation (2) for pure *bulk* SOTs to the data in Fig. 3b. To check if additionally interfacial torques play a role, the fit equation was extended to take into account an additional interfacial SOTs [19]. Accordingly, we fit our data with a combination of *bulk* and interfacial SOTs [16,19]:

$$b_{SOT}^{\theta}(\Phi = 0^{\circ}) = \frac{\Gamma_0^{\parallel}}{2} sin(2\theta_0) + T_0^{\parallel} + T_2^{\parallel} sin^2(\theta_0) \quad (5)$$

$$b_{SOT}^{\theta}(\Phi = 90^{\circ}) = -\frac{\Gamma_0^{\perp}}{2} sin(2\theta_0) - \cos(\theta_0)(T_0^{\perp} + T_2^{\perp} sin^2(\theta_0)) \quad (6)$$

Where $T_i^{\parallel}$ and $T_i^{\perp}$ are the i^{th} order components of the longitudinal and transverse components of SOTs from the interface. Fig. 3b shows the resulting fit of the interfacial SOTs.

To finally check if the key feature of *bulk* SOTs, namely the opposite behavior for $\Phi = 0°$ and $\Phi = 90°$ is universally present or a random occurrence by chance at 175 K (the data shown in Fig. 3), we investigate the temperature dependence. By extracting Γ_0 from each fit, the fundamental magnitude of *bulk* SOTs in Fe_3GeTe_2 can be determined as a function of temperature as shown in Fig. 4. As visible in the temperature dependence, the behavior of $\Gamma_0 * \cos(2\Phi)$ exhibits consistently at all temperatures opposite behavior for $\Phi = 0°$ and $\Phi = 90°$ in line with the prediction for *bulk* SOTs. Note that the fits for Γ_0 were done independently for $\Phi = 0°$ and $\Phi = 90°$ so that one could easily determine if the temperature dependence were qualitatively different for both orientations. However here we see that for both orientations the largest values for Γ_0 occur at the lowest temperatures and then decrease to lower values for temperatures up to 150K before increasing again and peaking around 215 K. Note that the reduction of Γ_0 at even higher temperatures approaching the Curie temperature (230 K) is expected as the magnetic order is lost and at elevated temperature close to the Curie temperature inhomogeneous properties and domain formation can make the analysis less robust. The complex behavior of Γ_0 at elevated temperatures could thus be related to the multi-step switching indicating domain formation shown in Fig. 1b. We note that at higher temperatures the error bars are smaller as the magnetization can be tilted with our maximum

available vector field of 5 T to higher angles and a wider θ_0 angle range can be investigated and fitted since the anisotropy decreases with temperature.

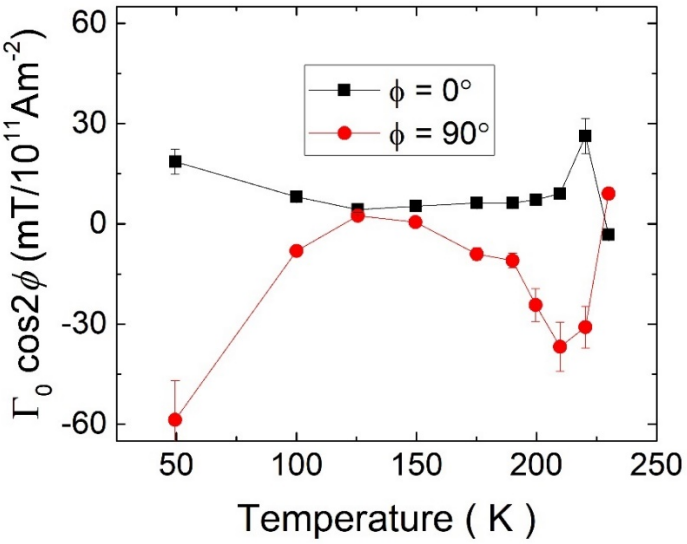

Figure 4. The extracted bulk SOT parameter Γ_0*cos(2Φ) as a function of the temperature showing the opposite sign for the Φ = 0° and Φ = 90° data over the full temperature range.

In particular, the data shows that at low temperatures we measure very high values of b^{θ}_{SOT} of more than 50 mT/10^{11} Am^{-2}. Together with the very high interfacial SOTs found in Fe_3GeTe_2/Pt structures [7,8], this bodes well for efficient switching of the magnetization in this material by combined bulk and interfacial torques.

In the following, we discuss the possible origins of the SOTs that we measure. In [16] a SOT mechanism related to a broken inversion symmetry of the structure is introduced. While the polar angular dependences found at the different temperatures indicate a dominating bulk origin of the torques, we see that the temperature dependence does show some deviations from the strict proportionality expected from eq. 6 and the absolute values for Φ = 0° and Φ = 90° shown in Fig. 4 do not always fully coincide. This indicates that additional higher order torques that can for instance be induced by uniaxial strain can play a role, highlighting the breadth of new torques that can contribute due to our identified bulk mechanisms. Furthermore, we see that fits of the polar angular dependence (Fig. 3) indicate additional

interfacial torques beyond the intrinsic *bulk* torque can be present. To check why interfacial torques can occur, even though the Fe_3GeTe_2 device that is measured is in principle a bulk device with a thickness of 35 nm, where no net interfacial torques due to the spin Hall effect or the inverse spin-galvanic effect [5,20] are expected, we consider surface oxidation. Overall, this device has been exposed to air < 12 hours and literature reports a natural oxidation layer on an exfoliated flake within a time scale of 14 hours [21,22]. The presence of an oxide layer on the surface exposed to air is confirmed by TEM (see supplementary material fig. S3) and thus interfacial SOTs can appear. So we find that in our Fe_3GeTe_2 device clear evidence for a theoretically reported *bulk* SOT based on the crystal symmetry breaking [16] and on the other hand an additional interfacial SOT are enabled by local surface oxidation. Mitigation of this surface contribution lies beyond the scope of this paper as either increased sample thickness or complete removal of the oxidation layer are the main options. The first is naturally non-trivial and the second results in drastic sample heating from large current densities. A third possible contribution to the measured SOTs could be Oersted fields, which are additional magnetic fields, which arise due to the current flow and can mimic a field-like torque symmetry. Assuming that the Fe_3GeTe_2 flake is a homogeneous conductor, the Oersted field is zero in the center of the flake and rises in magnitude at the edges, pointing counterclockwise in the *yz*-plane [23]. Thus, it points in opposite *y*-directions at the top and bottom of the flake and cancels to zero. If we assume that the Fe_3GeTe_2 flake has become a heterogeneous conductor due to possible interfaces, the current flow in the z-direction becomes asymmetric and hence also the Oersted field. In the less conducting areas, this Oersted field can be estimated by $H_{Oe} = \mu_0 j_C/(2\pi r)$ according to the Biot-Savart law for an infinite long straight conductor with r the distance from the conductor. Therefore, exactly at the interfaces to less conducting areas e.g. at the top of the flake the Oersted field becomes maximal. However, given that we probe the bulk of the flake, the contribution of the Oersted field will be negligible compared to the measured torque values.

In order to quantify the *bulk* SOT from a theoretical perspective, we employ the microscopic first-principles framework to compute the anti-damping SOT within the Kubo linear response theory for the Fe_3GeTe_2 *bulk* crystal (details are given in the Supplementary Note 6). As bulk Fe_3GeTe_2 maintains inversion symmetry the SOT vanishes globally [24]. However, each layer separately exhibits a non-vanishing SOT [25] which may lead to the non-vanishing effect observed experimentally. Instances where inversion symmetry is broken have also been observed [26]. If we decompose the unit cell into the A and B layers of Fe_3GeTe_2 (Fig. S5 of the supporting material) the top and bottom Fe atoms of the A-layer experience an equal in magnitude but opposite in sign SOT for an out-of-plane magnetization. However, once the magnetization is tilted away from the out-of-plane direction the SOT for each layer does not cancel out separately. From first principles, the estimated magnitude of the SOT per layer with a magnetization angle of $\theta = 30°$ from the z axis, and $\varphi = 55°$ from the current direction of is $2.19\, mT/(10^{11} Am^{-2})$ and similar order to that found experimentally (Fig. 3b at θ_0=30°, Φ = 55°). A further analysis of the origins of the bulk SOT is presented in supplementary Note 11.

3. Conclusion

In summary, we have measured SOTs in a pure Fe_3GeTe_2 flake with very large magnitudes of more than 50 mT/10^{11} Am^{-2}. From a symmetry analysis we can identify the predicted bulk SOTs that result from the particular crystalline structure of the Fe_3GeTe_2 that we determine by TEM imaging. In addition, we find that additional interfacial SOTs are present that result likely from surface effects such as observed oxidation. Ab initio calculations confirm that the layer resolved *bulk* SOT is of the same order of magnitude as the experiment. We thus demonstrate that the *bulk* SOTs that are a unique property of certain van der Waals materials such as Fe_3GeTe_2 yield very efficient magnetization manipulation due to high effective fields. The bulk SOTs are independent of the thickness of the material and thus comparatively thick layers with good thermal stability of the magnetic states can be used. Combined with the

possibility of simple device design with just a single material without any additional materials and layers, our findings lay the foundations for a new paradigm of 2D materials spin-orbitronic devices.

Supporting Information

Supporting Information is available from the Wiley Online Library or from the author.

Acknowledgements

The work at JGU Mainz was funded by the Deutsche Forschungsgemeinschaft (DFG, German Research Foundation) – TRR 173 – 268565370 (projects A01 and B02), the EU (FET-Open grant agreement no. 863155 (s-Nebula), ERC Synergy grant agreement no. 856538 (3D MAGiC), and the Research Council of Norway (QuSpin Center 262633). T.S., D.G., and Y.M. gratefully acknowledge the Jülich Supercomputing Centre for providing computational resources and Deutsche Forschungsgemeinschaft (DFG, German Research Foundation) – TRR 173 – 268565370 (project A11), TRR 288 – 422213477 (project B06).

References

(1) Huang, B.; Clark, G.; Navarro-Moratalla, E.; Klein, D. R.; Cheng, R.; Seyler, K. L.; Zhong, D.; Schmidgall, E.; McGuire, M. A.; Cobden, D. H.; Yao, W.; Xiao, D.; Jarillo-Herrero, P.; Xu, X. Layer-Dependent Ferromagnetism in a van Der Waals Crystal down to the Monolayer Limit. *Nature* **2017**, *546* (7657), 270–273. https://doi.org/10.1038/nature22391.

(2) Gong, C.; Zhang, X. Two-Dimensional Magnetic Crystals and Emergent Heterostructure Devices. *Science*. **2019**, *363* (6428), eaav4450. https://doi.org/10.1126/science.aav4450.

(3) Gong, C.; Li, L.; Li, Z.; Ji, H.; Stern, A.; Xia, Y.; Cao, T.; Bao, W.; Wang, C.; Wang, Y.; Qiu, Z. Q.; Cava, R. J.; Louie, S. G.; Xia, J.; Zhang, X. Discovery of Intrinsic Ferromagnetism in Two-Dimensional van Der Waals Crystals. *Nature* **2017**, *546* (7657), 265–269. https://doi.org/10.1038/nature22060.

(4) Gibertini, M.; Koperski, M.; Morpurgo, A. F.; Novoselov, K. S. Magnetic 2D Materials and Heterostructures. *Nat. Nanotechnol.* **2019**, *14* (5), 408–419. https://doi.org/10.1038/s41565-019-0438-6.

(5) Manchon, A.; Železný, J.; Miron, I. M.; Jungwirth, T.; Sinova, J.; Thiaville, A.; Garello, K.; Gambardella, P. Current-Induced Spin-Orbit Torques in Ferromagnetic and Antiferromagnetic Systems. *Rev. Mod. Phys.* **2019**, *91* (3), 35004. https://doi.org/10.1103/RevModPhys.91.035004.

(6) Ostwal, V.; Shen, T.; Appenzeller, J. Efficient Spin-Orbit Torque Switching of the Semiconducting Van Der Waals Ferromagnet Cr2Ge2Te6. *Adv. Mater.* **2020**, *32* (7), 1906021. https://doi.org/https://doi.org/10.1002/adma.201906021.

(7) Alghamdi, M.; Lohmann, M.; Li, J.; Jothi, P. R.; Shao, Q.; Aldosary, M.; Su, T.; Fokwa, B. P. T.; Shi, J. Highly Efficient Spin–Orbit Torque and Switching of Layered Ferromagnet Fe3GeTe2. *Nano Lett.* **2019**, *19* (7), 4400–4405. https://doi.org/10.1021/acs.nanolett.9b01043.

(8) Wang, X.; Tang, J.; Xia, X.; He, C.; Zhang, J.; Liu, Y.; Wan, C.; Fang, C.; Guo, C.; Yang, W.; Guang, Y.; Zhang, X.; Xu, H.; Wei, J.; Liao, M.; Lu, X.; Feng, J.; Li, X.; Peng, Y.; Wei, H.; Yang, R.; Shi, D.; Zhang, X.; Han, Z.; Zhang, Z.; Zhang, G.; Yu, G.; Han, X. Current-Driven Magnetization Switching in a van Der Waals Ferromagnet Fe3GeTe2. *Sci. Adv.* **2019**, *5* (8), eaaw8904. https://doi.org/10.1126/sciadv.aaw8904.

(9) Verchenko, V. Y.; Tsirlin, A. A.; Sobolev, A. V; Presniakov, I. A.; Shevelkov, A. V. Ferromagnetic Order, Strong Magnetocrystalline Anisotropy, and Magnetocaloric Effect in the Layered Telluride Fe3−δGeTe2. *Inorg. Chem.* **2015**, *54* (17), 8598–8607. https://doi.org/10.1021/acs.inorgchem.5b01260.

(10) Fei, Z.; Huang, B.; Malinowski, P.; Wang, W.; Song, T.; Sanchez, J.; Yao, W.; Xiao, D.; Zhu, X.; May, A. F.; Wu, W.; Cobden, D. H.; Chu, J.-H.; Xu, X. Two-Dimensional Itinerant Ferromagnetism in Atomically Thin Fe3GeTe2. *Nat. Mater.* **2018**, *17* (9), 778–782. https://doi.org/10.1038/s41563-018-0149-7.

(11) Ding, B.; Li, Z.; Xu, G.; Li, H.; Hou, Z.; Liu, E.; Xi, X.; Xu, F.; Yao, Y.; Wang, W. Observation of Magnetic Skyrmion Bubbles in a van Der Waals Ferromagnet Fe3GeTe2. *Nano Lett.* **2020**, *20* (2), 868–873. https://doi.org/10.1021/acs.nanolett.9b03453.

(12) Wu, Y.; Zhang, S.; Zhang, J.; Wang, W.; Zhu, Y. L.; Hu, J.; Yin, G.; Wong, K.; Fang, C.; Wan, C.; Han, X.; Shao, Q.; Taniguchi, T.; Watanabe, K.; Zang, J.; Mao, Z.; Zhang, X.; Wang, K. L. Néel-Type Skyrmion in WTe2/Fe3GeTe2 van Der Waals Heterostructure. *Nat. Commun.* **2020**, *11* (1), 3860. https://doi.org/10.1038/s41467-020-17566-x.

(13) Park, T.-E.; Peng, L.; Liang, J.; Hallal, A.; Yasin, F. S.; Zhang, X.; Song, K. M.; Kim, S. J.; Kim, K.; Weigand, M.; Schütz, G.; Finizio, S.; Raabe, J.; Garcia, K.; Xia, J.; Zhou, Y.; Ezawa, M.; Liu, X.; Chang, J.; Koo, H. C.; Kim, Y. D.; Chshiev, M.; Fert, A.; Yang, H.; Yu, X.; Woo, S. Néel-Type Skyrmions and Their Current-Induced Motion in van Der Waals Ferromagnet-Based Heterostructures. *Phys. Rev. B* **2021**, *103* (10), 104410. https://doi.org/10.1103/PhysRevB.103.104410.

(14) León-Brito, N.; Bauer, E. D.; Ronning, F.; Thompson, J. D.; Movshovich, R. Magnetic Microstructure and Magnetic Properties of Uniaxial Itinerant Ferromagnet Fe3GeTe2. *J. Appl. Phys.* **2016**, *120* (8), 83903. https://doi.org/10.1063/1.4961592.

(15) Deng, Y.; Yu, Y.; Song, Y.; Zhang, J.; Wang, N. Z.; Sun, Z.; Yi, Y.; Wu, Y. Z.; Wu, S.; Zhu, J.; Wang, J.; Chen, X. H.; Zhang, Y. Gate-Tunable Room-Temperature Ferromagnetism in Two-Dimensional Fe3GeTe2. *Nature* **2018**, *563* (7729), 94–99. https://doi.org/10.1038/s41586-018-0626-9.

(16) Johansen, Ø.; Risinggård, V.; Sudbø, A.; Linder, J.; Brataas, A. Current Control of Magnetism in Two-Dimensional Fe3GeTe2. *Phys. Rev. Lett.* **2019**, *122* (21), 217203. https://doi.org/10.1103/PhysRevLett.122.217203.

(17) Lee, J. W.; Park, J. Y.; Yuk, J. M.; Park, B.-G. Spin-Orbit Torque in a Perpendicularly Magnetized Ferrimagnetic Tb-Co Single Layer. *Phys. Rev. Appl.* **2020**, *13* (4), 44030. https://doi.org/10.1103/PhysRevApplied.13.044030.

(18) Zheng, S. Q.; Meng, K. K.; Liu, Q. B.; Chen, J. K.; Miao, J.; Xu, X. G.; Jiang, Y. Disorder Dependent Spin–Orbit Torques in L10 FePt Single Layer. *Appl. Phys. Lett.* **2020**, *117* (24), 242403. https://doi.org/10.1063/5.0028815.

(19) Garello, K.; Miron, I. M.; Avci, C. O.; Freimuth, F.; Mokrousov, Y.; Blügel, S.; Auffret, S.; Boulle, O.; Gaudin, G.; Gambardella, P. Symmetry and Magnitude of Spin–Orbit Torques in Ferromagnetic Heterostructures. *Nat. Nanotechnol.* **2013**, *8* (8), 587–593. https://doi.org/10.1038/nnano.2013.145.

(20) Manchon, A.; Belabbes, A. Chapter One - Spin-Orbitronics at Transition Metal Interfaces; Camley, R. E., Stamps, R. L. B. T.-S. S. P., Eds.; Academic Press, 2017; Vol. 68, pp 1–89. https://doi.org/https://doi.org/10.1016/bs.ssp.2017.07.001.

(21) Kim, D.; Park, S.; Lee, J.; Yoon, J.; Joo, S.; Kim, T.; Min, K.; Park, S.-Y.; Kim, C.; Moon, K.-W.; Lee, C.; Hong, J.; Hwang, C. Antiferromagnetic Coupling of van Der Waals Ferromagnetic Fe3GeTe2. *Nanotechnology* **2019**, *30* (24), 245701. https://doi.org/10.1088/1361-6528/ab0a37.

(22) Park, T.-E.; Peng, L.; Liang, J.; Hallal, A.; Sami Yasin, F.; Zhang, X.; Jong Kim, S.; Song, K. M.; Kim, K.; Weigand, M.; Schuetz, G.; Finizio, S.; Raabe, J.; Garcia, K.; Xia, J.; Zhou, Y.; Ezawa, M.; Liu, X.; Chang, J.; Koo, H. C.; Duck Kim, Y.; Chshiev, M.; Fert, A.; Yang, H.; Yu, X.; Woo, S. Néel-Type Skyrmions and Their Current-Induced Motion in van Der Waals Ferromagnet-Based Heterostructures. *arXiv:1907.01425*. July 1, 2019, p arXiv:1907.01425.

(23) Ho, P.; Zhang, J.; Bono, D. C.; Chen, J.; Ross, C. A. Oersted Field and Spin Current Effects on Magnetic Domains in [Co/Pd]15 Nanowires. *IEEE Trans. Magn.* **2016**, *52* (6), 1–6. https://doi.org/10.1109/TMAG.2016.2526972.

(24) Zhang, K.; Han, S.; Lee, Y.; Coak, M. J.; Kim, J.; Hwang, I.; Son, S.; Shin, J.; Lim, M.; Jo, D.; Kim, K.; Kim, D.; Lee, H.-W.; Park, J.-G. Gigantic Current Control of Coercive Field and Magnetic Memory Based on Nanometer-Thin Ferromagnetic van Der Waals Fe3GeTe2. *Adv. Mater.* **2021**, *33* (4), 2004110. https://doi.org/https://doi.org/10.1002/adma.202004110.

(25) Saunderson, T. G.; Go, D.; Blügel S.; Kläui M.; Mokrousov, Y.; "Hidden interplay of current-induced spin and orbital torques in bulk Fe_3GeTe_2", arXiv:2204.13052 (2022)

(26) Chakraborty, A.; Srivastava, A. K.; Sharma, A. K.; Gopi, A. K.; Mohseni, K.; Ernst, A.; Deniz, H.; Hazra, B. K.; Das, S.; Sessi, P.; Kostanovskiy, I.; Ma, T.; Meyerheim, H. L.; Parkin, S. S. P., "Magnetic Skyrmions in a Thickness Tunable 2D Ferromagnet from a Defect Driven Dzyaloshinskii–Moriya Interaction", Advanced Materials **34**, 2108637 (2022)